Available online at www.eccomasproceedia.org
Eccomas Proceedia COMPDYN (2025) 5 2-5 41

ECCOMAS
Proceedia

COMPDYN 2025
10th ECCOMAS Thematic Conference on
Computational Methods in Structural Dynamics and Earthquake Engineering
M. Papadrakakis, M. Fragiadakis (eds.)
Rhodes Island, Greece, 15-18 June 2025

THE DYNAMIC IMPACT OF SURGE WAVES ON MULTI-COLUMN BRIDGE BENTS

S. M. Hadi Moosavian[1], Shooka Karimpour[1], and Stavroula Pantazopoulou[1]

[1] Department of Civil Engineering, York University
4700 Keele St, Toronto, ON M3J 1P3, Canada
e-mail: smhadim@yorku.ca, pantazo@yorku.ca, shooka.karimpour@lassonde.yorku.ca

Abstract

Among the intensifying natural hazards, flash floods and tsunami waves have emerged as some of the most destructive events, significantly impacting transportation infrastructure, particularly bridges. While structural engineering studies have traditionally focused on earthquake loading and the seismic performance of bridge structures, the dynamic impact of severe transient surge waves—such as tsunami waves and flash floods—can adversely affect the serviceability and seismic performance, posing a critical threat to bridges. This study investigates the dynamic loads exerted by surge waves on bridge piers using hydrodynamic modeling. Specifically, the effect of piers interaction in multi-column bridge configurations on the wave load was analyzed. Moreover, the effect of spacing between columns on the resultant overturning moment was examined. The time history of the wave load on bridge piers shows the meaningful interaction of columns on the resultant force. Moreover, the dynamic nature of the flash flood/tsunami load was discussed. These effects, however, are often overlooked in the calculation of hydrodynamic loads in structural design codes.

Keywords: Multicolumn Bridge System, Hydrodynamic Load, Flash Flood, Tsunami, Dynamic Loading, Column Spacing.

Peer-review under responsibility of the organizing committee of COMPDYN 2025.
doi: 10.7712/120125.12816.26068

1 INTRODUCTION

The shifting climate has increased the frequency and intensity of extreme weather events, including coastal storm surges and sudden floods [1], [2]. While structural engineering research has traditionally prioritized earthquake loading and seismic performance, severe transient surge waves—such as tsunamis and flash floods—pose a critical threat to bridge structures. These events can compromise both serviceability and seismic resilience [3], [4]. As a result, these changes may lead to significant revisions in the flood-related pressures outlined in design regulations [5]. During floods or tsunamis, the rapid surge in water pressure and volume, coupled with soil scouring and debris impact on structural components, can lead to sudden bridge failure. Wardhana et al. [6] analyzed 503 cases of bridge failures in the U.S. from 1989 to 2000, identifying hydraulic loading—primarily due to flash floods—as the leading cause of bridge collapses.

In recent decades, both numerical and experimental studies have investigated the impact of breaking waves on bridge piers. In 2009, Arnason et al. [7] examined experimentally tsunami-structure interactions, analyzing how tsunami waves affect structures with different cross-sections, particularly the impact of a tsunami bore on a vertical column. Similarly, Nouri et al. [8] explored the effects of dam-break waves on structures with square, diamond, and circular cross-sections, assessing bore height and flow velocities along a flume. With advancements in computational modeling, numerical studies have also expanded. Chen et al. numerically investigated sinusoidal wave interactions with a vertical cylinder, representing a typical offshore wind turbine foundation [9]. In 2021, Peng et al. [10] numerically examined the impact of a dam-break induced flood on a solitary downstream structure, focusing on the flow regime, temporal variations, and impact pressure distribution. Additionally, Istrati and Hasanpour [11] conducted numerical simulations to investigate dam-break-induced extreme flooding and its effects on bridge superstructures.

Despite the extensive research on riverine bridge flooding, most studies primarily focus on single-column bridge bents. Although multi-column bridge bents occur commonly in bridge engineering, only limited data exists regarding their response to flood loading. This study investigates the impact of flash floods on multi-column bridges, comparing the forces exerted on the sequence of the columns within a bent, to those exerted on single-column bridge bents. Additionally, the paper examines how the spacing between the columns in a bent, and the wave intensity affect the forces acting on the bridge piers.

2 PROBLEM DEFINITION AND MODEL DESCRIPTION

The primary objective of this research was to examine the impact of flash floods and tsunami waves on multi-column bridge systems. From a hydrodynamic perspective, both phenomena share similar characteristics, exhibiting transient, highly turbulent flow regimes with high Froude numbers. Furthermore, Chanson [12] demonstrated that the flow characteristics of dam-break waves align well with field data by comparing them with visual images of broken tsunami waves. Due to this similarity, many studies have used dam-break waves to model surge waves [13]–[15]. Accordingly, this study employed a dam-break wave on a wet bed—where water is suddenly released following the abrupt removal of a reservoir gate—to simulate flash floods and tsunamis.

For the needs of the hydrodynamic simulation, the structure was assumed to undergo minimal deformation, with negligible effects on wave impact. Therefore, any feedback from the structure on the wave was neglected, and the pier was modeled as a sequence of rigid, massless piles of orthogonal cross section. The simulations were performed using OpenFOAM (Open-

Source Field Operation and Manipulation), an open-source computational platform, employing a Large Eddy Simulation (LES) approach. Further details on the LES method can be found in [16] and [17].

The simulations employed the LES-filtered momentum equations as the governing equations, solving them in all three spatial directions. A detailed discussion of the solver, governing equations, validation of the modeling approach against experimental studies, and mesh sensitivity analysis can be found in [5].

Figure 1 presents a schematic representation of the 3D numerical models. Flash flood modeling was conducted by simulating dam-break waves while considering multi-column bridge systems with various configurations. To ensure comparability, key geometric properties remained consistent, and square pier sections were used with the same size (D_p). The reservoir length was set to L_1=120 m to prevent the reflection of a negative wave propagating in the reservoir before the bore reaches the pier structure. The distance between the dam and the central bridge pier (L_0) was set to 30 m, while the channel width (W) was maintained at 10 m. Given the problem's symmetry, only half of the channel was modeled in the transverse direction, with a symmetry boundary condition applied along the channel's centerline. To mitigate wave reflections at the downstream end, an outlet boundary condition was implemented.

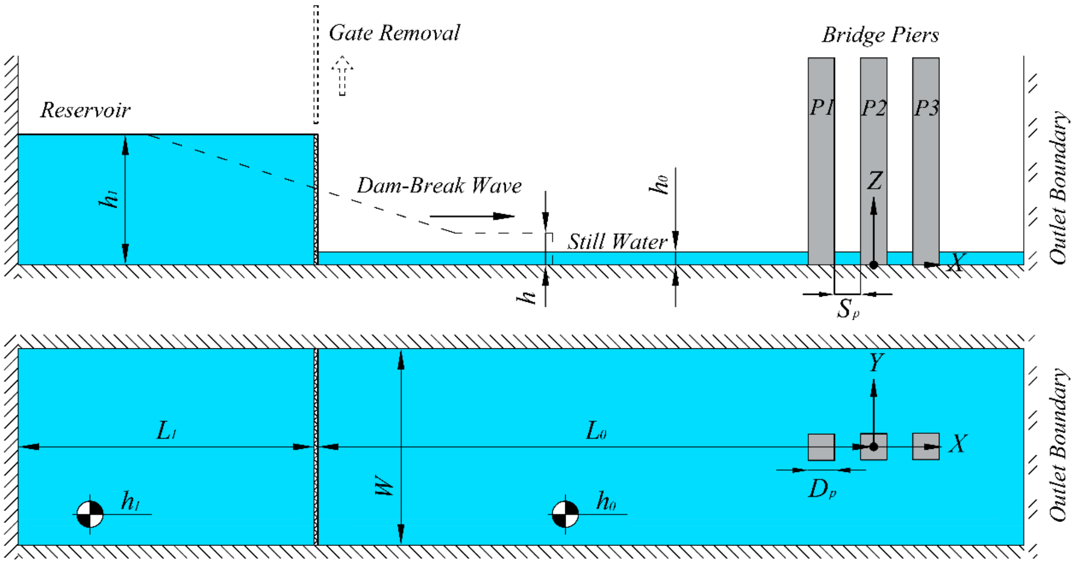

Figure 1: Schematic representation of numerical model; top: side view, bottom: plan view

The key parameters defining a dam-break wave on a wet bed are the reservoir height (h_1) and the still water depth (h_0), both of which significantly influence the resulting wave dynamics. A rapid estimation of dam-break wave characteristics can be obtained using the Method of Characteristics (MOC), a simplified approach developed by [18], [19]. While less detailed than dynamic modeling, MOC provides reasonably accurate estimates of wave properties such as stream height and velocity. The detailed discussion for MOC can be also found in [5]. Accordingly, the primary characteristics of the dam-break wave—including wave celerity (C), wave velocity (V), and stream height (h)—were calculated and are presented in Table 1.

Table 1 provides a summary of the models simulated in this study. It included a comparison between multi-column bent (M) and single-column bent (S) systems, as well as an exploration of the effects of the spacing between columns (S_p) and wave intensity. The models, detailed in Table 1, are identified by codes that denote multi or singe column bents (M and S), the wave intensity (I1 or I2) and the clear spacing (in m) between successive columns (1, 2, 3). The last two models, S-I1 and S-I2, represented single-column systems and served as the benchmark for comparison. Additionally, the mesh configurations and refinement across all models aligned with the scheme outlined in [5].

Table 1: Description of simulated models (For definition of the symbols also see Figure 1)

Case	h_1 (m)	h_0 (m)	h (m)	V (m/s)	C (m/s)	D_p (m)	S_p (m)
M-I1-1	5.00	0.50	1.98	5.20	6.96	1.00	1.00
M-I1-2	5.00	0.50	1.98	5.20	6.96	1.00	2.00
M-I1-3	5.00	0.50	1.98	5.20	6.96	1.00	3.00
M-I2-1	6.00	0.50	2.22	5.99	7.73	1.00	1.00
S-I1	5.00	0.50	1.98	5.20	6.96	1.00	N.A.
S-I2	6.00	0.50	2.22	5.99	7.73	1.00	N.A.

3 RESULTS AND DISCUSSIONS

This section discusses the forces and overturning moments exerted on piers under different scenarios. A comparison was made between single-column and multi-column bridge bents, followed by an analysis of the effect of the spacing between piers in the direction of the river flow. Finally, a brief discussion on the nature of surge wave impact was presented. The force and overturning moment time history were determined by considering the pressure distribution across the upstream and downstream faces of the bridge piers.

All time histories in this section were presented using a shifted time variable (t^*), where the elapsed time since the onset of the dam-break wave is adjusted by the nominal arrival time of the wave at the first column (P1 in Figure 1). The arrival time was determined using the celerity (C) computed based on MOC and was provided in Table 1. With this adjustment, t^* is set to zero at the moment of impact of the dam-break wave.

3.1 Comparison of multicolumn and single column systems

Figure 2 compares the resultant forces on multicolumn (M-I1-1) and single-column (S-I1) bridge systems. In Figure 2a, results for the single pier were presented, while Figure 2b displayed results for the multicolumn case, where forces on P1, P2, and P3 (as defined in Figure 1) were shown separately. As seen in Figure 2b, due to the varying arrival times of the surge wave at different piers, force peaks occurred at different time steps. To account for this, the total force acting on the bridge bent was calculated by summing the forces applied to all pier columns and is shown in Figure 2c.

Comparing P1 in M-I1-1 to the single pier in S-I1, the first two peaks at $t^* = 0.05$ s and 0.60 s—measuring 36 kN and 46 kN, respectively—were consistent, indicating that upstream conditions remained unchanged in the multicolumn case at initial stages. However, the third peak was influenced by pier interactions. While the single-column case experienced a peak force of 52 kN at $t^* = 1$ s, the P1 pier in M-I1-1 reached 47 kN at $t^* = 1.3$ s. Additionally, in the pseudo-steady state, calculated as the average force over the last 5 seconds of the simulation, S-I1 experienced a force of 40 kN, whereas P1 in M-I1-1 experienced 33 kN. The effects of pier interactions were further illustrated in Figure 3, which depicts the water profile along the symmetry axis at $t^* = 1.3$ s. While the upstream conditions for P1 in M-I1-1 remained unchanged compared to S-I1, downstream fluctuations were influenced by pier interactions.

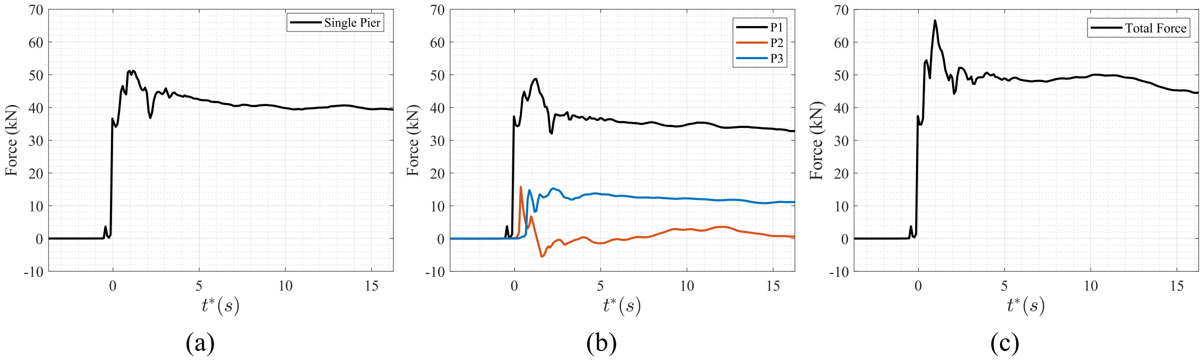

Figure 2: The time history of resultant force; (a) single column case (S-I1), (b) individual columns in multi-column case (M-I1-1), (c) accumulated force in M-I1-1

The effects of pier interactions were more pronounced for P2 and P3, where the resultant forces were significantly decreased as compared to the single-pier case. P2 in M-I1-1 peaked at 15.7 kN and had a pseudo-steady force of 2 kN. Similarly, P3 in M-I1-1 experienced a maximum force of 15 kN and a pseudo-steady force of 11 kN. The key difference between P2 and P3 was that while both sides of P2 were affected by pier interactions, the downstream side of P3 remained largely unaffected. In the case of P2, pier interactions and water accumulation on the downstream side led to a near-zero resultant force in the pseudo-steady state.

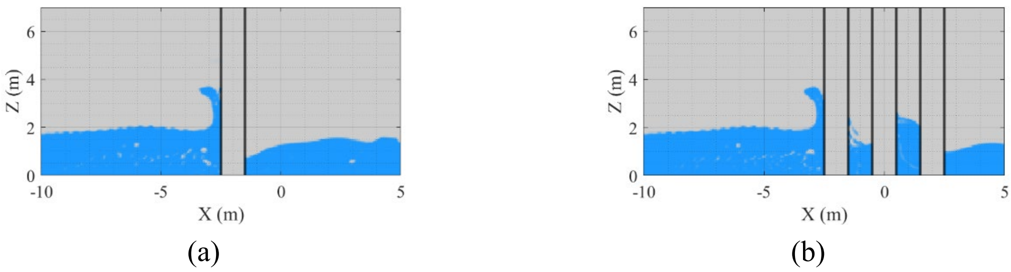

Figure 3: Water profile along the symmetry axis at t^*= 1.3 s; (a) S-I1 (single column case), (b) M-I1-1 (multicolumn case)

While the individual forces on P1, P2, and P3 are important, the total force acting on the bridge bent is also critical—especially when all bent columns share the same foundation. Figure 2c presents the accumulated force from P1 to P3, considering the different arrival times of the wave. The maximum accumulated force reached 66 kN, which is 40% higher than the peak force on P1 and 25% higher than that in S-I1. The pseudo-steady force also averaged 47 kN. Thus, the total force transferred to the foundation exceeded the maximum force experienced by any individual bent column and also by the single column pier.

Changing the wave intensity did not affect the conclusions of the previous discussion, as shown in Figure 4. In P1 of –M-I2-1, the first two peaks remained unchanged from the single-column case (S-I2), reaching 45 kN and 58 kN at t^* = 0.04 s and 0.8 s, respectively. However, the third peak in P1 of –M-I2-1 decreased by 10% compared to single pier (S-I2), aligning with the comparisons presented for previous wave intensity (M-I1). For the middle column, the results for P2 of –M-I2-1 were nearly identical to those of P2 of –M-I1-1, with a peak force of 15 kN and a pseudo-steady force of 1 kN. Additionally, P3 of –M-I2-1 exhibited a peak force of 22 kN and a pseudo-steady force of 18 kN, reflecting an average decrease of 70% compared to P1 of M-I2-1, consistent with the trends observed in the M-I1 cases.

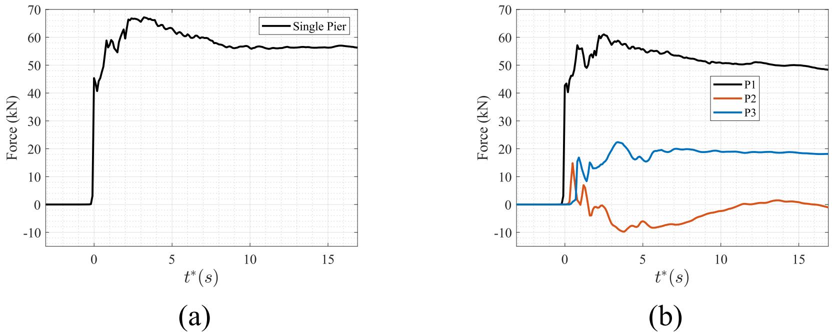

Figure 4: The time history of resultant force of the more intense wave scenario; (a) single column bent (S-I2), (b) individual columns in multicolumn bent (M-I2-1)

3.2 Influence of pier spacing on hydrodynamic actions

As discussed in the previous section, water-pier interactions in a multicolumn system can significantly influence the resultant forces. This section examined the effect of pier spacing by comparing the overturning moments in three cases: M-I1-1 (1 m clear spacing between columns in a bent (S_p)), M-I1-2 (S_p=2 m), and M-I1-3 (S_p=3 m), as depicted in Figure 5. While the first pier (P1) was not significantly affected by spacing, the forces on P2 and P3 exhibited notable variations.

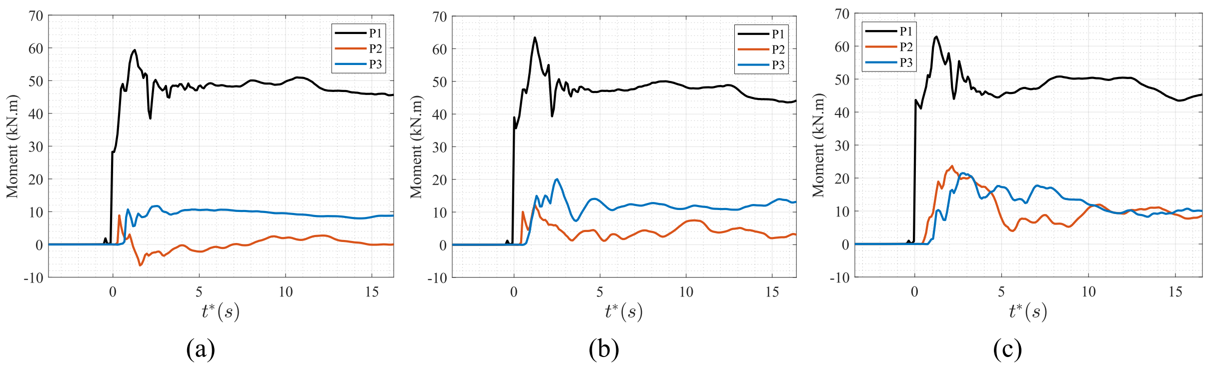

Figure 5: The time history of resultant overturning moment; (a) M-I1-1, (b) M-I1-2, (c) M-I1-3

The peak overturning moments for P1 were 60 kN·m, 63 kN·m, and 62 kN·m in the M-I1-1, M-I1-2, and M-I1-3 models, respectively, showing minimal changes. The pseudo-steady moment for P1 also remained relatively unchanged across all models, averaging 45 kN·m, as presented in Table 2.

Table 2: Summary of the results of the multicolumn cases

Case	Peak Moment (kN·m)	Pseudo steady Moment (kN·m)	Peak Moment (kN·m)	Pseudo steady Moment (kN·m)	Peak Moment (kN·m)	Pseudo steady Moment (kN·m)
	P1		P2		P3	
M-I1-1	60	46	9	1	6	8
M-I1-2	63	44	11	4	21	12
M-I1-3	62	45	23	11	21	10

In contrast, the peak moment for P2 increased from 9 kN·m in M-I1-1 to 11 kN·m in M-I1-2 and 23 kN·m in M-I1-3. The pseudo-steady moment for P2 also showed significant variation, rising from 1 kN·m in M-I1-1 to 11 kN·m in M-I1-3. A similar trend was observed for P3, where the peak overturning moment increased from 6.2 kN·m in M-I1-1 to 21 kN·m in M-I1-3. However, changes in the pseudo-steady moment for P3 were minimal.

These differences in the overturning moments of P2 and P3 can be further understood by examining Figure 6, which presents the water profile from both the side view (along the symmetry axis) and the top view (showing half of the model due to symmetry) at t^* = 2.2 s. While the upstream and downstream water profiles around P1 remained nearly identical across all models, the profiles around P2 and P3 were notably influenced by pier-water interactions.

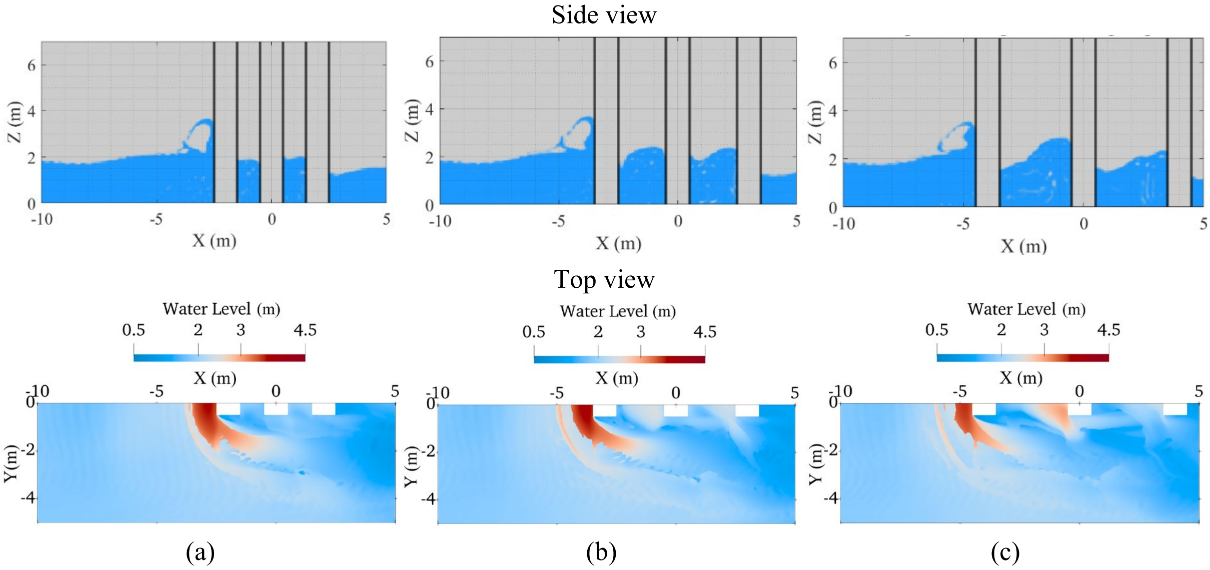

Figure 6: Water profile from side and top views at t^* = 2.2 s; (a) M-I1-1, (b) M-I1-2, (c) M-I1-3

3.3 Nature of hydrodynamic load

While variations in the magnitude of hydrodynamic forces are observed across different design codes [5], these codes consistently treat hydrodynamic forces as static loads [20]–[22]. For instance, Baiguera et al. [23] developed a procedure for performing nonlinear pushover analysis of flow-induced loads based on ASCE 7-16. Additionally, several studies have considered flood and tsunami loads as static forces [24]–[26].

However, an examination of the time history of forces exerted on bridge bents—including both single and multicolumn configurations—revealed the inherently dynamic nature of wave loads. To investigate this further, frequency analysis can provide valuable insights. Figure 7 presents the frequency spectrum of the force acting on P1 in the M-I1-1 model. To focus on the primary wave impact, the force time history was analyzed within a window from t = 3.5 s to 7.5 s, where the most significant fluctuations occurred, as depicted in Figure 7. This means that the initial constant force (DC component) and the pseudo-steady-state section were excluded to focus solely on the dynamic component of the response. The sampling frequency was set to 200 Hz, and the Fourier spectrum was computed using MATLAB [27].

As shown in Figure 7, the first peak occurred at approximately fr = 1 Hz, followed by multiple peaks, indicating a frequency spectrum characteristic of a step force or a rectangular pulse force—an observation further supported by the time history diagram. According to structural dynamics principles, whether the force is considered a step load with a short rise time or a rectangular pulse with a long duration, the maximum ratio of dynamic response to static response for an ideal single-degree-of-freedom (SDOF) system is 2 [28]. Therefore, for an accurate assessment of structural response to flash flood loads, if dynamic analysis that considers the time history of hydrodynamic loads is not feasible, an amplification factor should be incorporated into static analyses. A precise determination of the amplification factor requires further hydrodynamic and structural analyses.

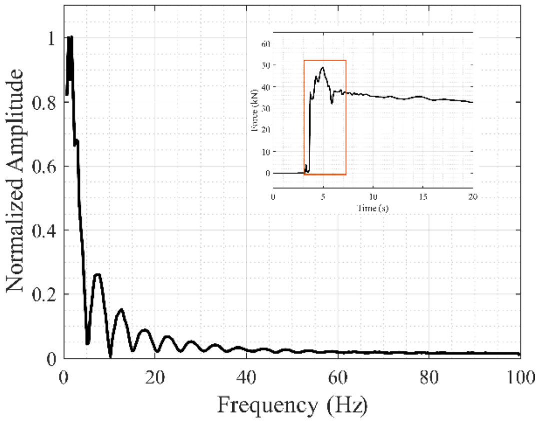

Figure 7: The frequency spectrum of the force time history acting on P1of M-I1-1

4 CONCLUSIONS

While the impact of flood- and tsunami-induced hydrodynamic loads on single-column bridge systems has been addressed in the literature and design codes, multi-column bridge systems have received less attention. This study investigated the hydrodynamic forces exerted on multi-column bridge bents by tsunami- and flash flood-induced surge waves.

The results showed that the leading bent column in the streamwise direction experienced a 10% decrease in hydrodynamic force compared to a single-column bent, while the downstream bent columns exhibited a significant reduction in force. However, the total force exerted on the multi-column bent was 25% higher than that on a single-column pier, highlighting important implications for foundation design. Furthermore, column spacing had a notable influence on the forces experienced by the downstream piers. Additionally, the study emphasized the necessity of considering the dynamic nature of tsunami- and flash flood-induced impacts in structural analyses.

REFERENCES

[1] Z. W. Kundzewicz, I. Pin'skwar, and G. R. Brakenridge, "Changes in river flood hazard in Europe: a review," *Hydrol. Res.*, vol. 49, no. 2, pp. 294–302, Apr. 2018, doi: 10.2166/NH.2017.016.

[2] W. R. Berghuijs, E. E. Aalbers, J. R. Larsen, R. Trancoso, and R. A. Woods, "Recent changes in extreme floods across multiple continents," *Environ. Res. Lett.*, vol. 12, no. 11, p. 114035, Nov. 2017, doi: 10.1088/1748-9326/AA8847.

[3] S. Qin, H. Wang, Z. Luo, S. Qin, H. Wang, and Z. Luo, "Recent hydraulic bridge failures in China: review and discussion," *Rev. la construcción*, vol. 21, no. 2, pp. 193–203, 2022, doi: 10.7764/RDLC.21.2.193.

[4] I. Ario *et al.*, "Investigation of Bridge Collapse Phenomena due to Heavy Rain Floods: Structural, Hydraulic, and Hydrological Analysis," *J. Bridg. Eng.*, vol. 27, no. 9, p.

04022073, Sep. 2022.

[5] S. M. H. Moosavian, S. Karimpour, and S. Pantazopoulou, “Comparative Analysis of Hydrodynamic Loads on Bridge Piers: Assessing Standards through Numerical Modeling,” *Can. J. Civ. Eng.*, Oct. 2024, doi: 10.1139/CJCE-2024-0145.

[6] K. Wardhana and F. C. Hadipriono, “Analysis of recent bridge failures in the United States,” *J. Perform. Constr. Facil.*, vol. 17, no. 3, pp. 144–150, Aug. 2003, doi: 10.1061/(ASCE)0887-3828(2003)17:3(144).

[7] H. Arnason, C. Petroff, and H. Yeh, “Tsunami Bore Impingement onto a Vertical Column,” *J. Disaster Res.*, vol. 4, no. 6, pp. 391–403, Dec. 2009, doi: 10.20965/JDR.2009.P0391.

[8] Y. Nouri, I. Nistor, D. Palermo, and A. Cornett, “Experimental Investigation of Tsunami Impact on Free Standing Structures,” *Coast. Eng. J.*, vol. 52, no. 1, pp. 43–70, 2010, doi: 10.1142/S0578563410002117.

[9] L. F. Chen, J. Zang, A. J. Hillis, G. C. J. Morgan, and A. R. Plummer, “Numerical investigation of wave–structure interaction using OpenFOAM,” *Ocean Eng.*, vol. 88, pp. 91–109, Sep. 2014, doi: 10.1016/J.OCEANENG.2014.06.003.

[10] L. Peng, T. Zhang, Y. Rong, C. Hu, and P. Feng, “Numerical investigation of the impact of a dam-break induced flood on a structure,” *Ocean Eng.*, vol. 223, p. 108669, Mar. 2021, doi: 10.1016/J.OCEANENG.2021.108669.

[11] D. Istrati and A. Hasanpour, “Numerical Investigation of Dam Break-Induced Extreme Flooding of Bridge Superstructures,” in *3rd International Conference on Natural Hazards & Infrastructure*, 2022.

[12] H. Chanson, “Tsunami Surges on Dry Coastal Plains: Application of Dam Break Wave Equations,” *Coast. Eng. J.*, vol. 48, no. 4, pp. 355–370, 2006, doi: 10.1142/S0578563406001477.

[13] A. J. Crespo, M. Gómez-Gesteira, and R. A. Dalrymple, “Modeling Dam Break Behavior over a Wet Bed by a SPH Technique,” *J. Waterw. Port, Coastal, Ocean Eng.*, vol. 134, no. 6, pp. 313–320, Nov. 2008.

[14] M. Rajaie *et al.*, “Experimental Investigations on Hydrodynamic Characteristics of Tsunami-Like Hydraulic Bores Impacting a Square Structure,” *J. Hydraul. Eng.*, vol. 148, no. 3, p. 04021061, Dec. 2021, doi: 10.1061/(ASCE)HY.1943-7900.0001965.

[15] P. Xie and V. H. Chu, “The forces of tsunami waves on a vertical wall and on a structure of finite width,” *Coast. Eng.*, vol. 149, pp. 65–80, Jul. 2019, doi: 10.1016/J.COASTALENG.2019.03.013.

[16] S. B. Pope, “Ten questions concerning the large-eddy simulation of turbulent flows,” *New J. Phys.*, vol. 6, no. 1, p. 35, Mar. 2004, doi: 10.1088/1367-2630/6/1/035.

[17] A. Venkateshwaran, Z. Li, and S. Karimpour, “Turbulent characteristics and anisotropy in breaking surge waves: A numerical study,” *Phys. Fluids*, vol. 35, no. 1, p. 15132, Jan. 2023, doi: 10.1063/5.0130657/2868052.

[18] H. Chanson, *Environmental Hydraulics for Open Channel Flows*, 1st ed. Oxford, UK: Elsevier Butterworth-Heinemann, 2004.

[19] H. Chanson, “Analytical Solution of Dam Break Wave with Flow Resistance:

Application to Tsunami Surges," vol. 137, Jan. 2005.

[20] "ASCE/SEI 7-22," *Minim. Des. loads Assoc. criteria Build. other Struct.*, 2022.

[21] "CSA S6:19," *Can. Highw. Bridg. Des. Code*, 2019.

[22] "EN 1991-1," *Eurocode 1 Actions Struct. Part 1-6 Gen. actions — Actions Dur. Exec.*, 2005.

[23] M. Baiguera, T. Rossetto, I. N. Robertson, and C. Petrone, "A Procedure for Performing Nonlinear Pushover Analysis for Tsunami Loading to ASCE 7," *J. Struct. Eng.*, vol. 148, no. 2, Feb. 2022, doi: 10.1061/(ASCE)ST.1943-541X.0003256.

[24] S. A. Argyroudis and S. A. Mitoulis, "Vulnerability of bridges to individual and multiple hazards- floods and earthquakes," *Reliab. Eng. Syst. Saf.*, vol. 210, p. 107564, Jun. 2021, doi: 10.1016/J.RESS.2021.107564.

[25] T. J. Carey, S. M. Asce, ; H Benjamin Mason, A. R. Barbosa, A. M. Asce, and M. H. Scott, "Multihazard Earthquake and Tsunami Effects on Soil–Foundation–Bridge Systems," *J. Bridg. Eng.*, vol. 24, no. 4, p. 04019004, Apr. 2019, doi: 10.1061/(ASCE)BE.1943-5592.0001353.

[26] A. Anisha, A. Jacob, R. Davis, and S. Mangalathu, "Fragility functions for highway RC bridge under various flood scenarios," *Eng. Struct.*, vol. 260, p. 114244, Jun. 2022, doi: 10.1016/J.ENGSTRUCT.2022.114244.

[27] "MATLAB-R2022b." The MathWorks Inc., Natick, Massachusetts, United States, 2022. [Online]. Available: https://www.mathworks.com

[28] A. K. Chopra, *Dynamics of Structures*, 5 th ed. Pearson, 2017.